Supporting Information

Baumgartner et al. 10.1073/pnas.1111408109

SI Text

Culture Conditions. Yeast cells adapt to growth on galactose more rapidly if they had prior exposure to galactose (1). Likewise, we have observed that cells respond to glucose more readily if they have been grown in glucose before, although the mechanism behind this observation is unknown. Because past growth conditions influence the dynamics of the response to changes in carbon source, in all of our experiments the initial cultures were started from single colonies inoculated into synthetic medium containing a mixture of galactose and glucose (1%/1%). As expected, we found that cells growing in this mixed medium exhibited diauxie (i.e., they metabolized the glucose in the medium before using the galactose). After an overnight incubation, the starter culture was diluted 1:100 into fresh 1%/1% medium. We determined that the glucose of the fresh culture became depleted, and *GAL1* expression was concomitantly induced, within 4 h of dilution. Using this culturing scheme, we were able to ensure that the cells used in our experiments had experienced both glucose and galactose in their recent past and could respond with maximum efficiency to either sugar.

Microfluidics Device. The microfluidic chip used in this study is an improved version of the device described in Bennett et al. (2) and is designed for the study of *Saccharomyces cerevisiae* cells in a defined microenvironment. This new device features a superior mixing system that leads to more reproducible output profiles of inducer compared with the previous design (Fig. S2) and methods to change the mixing ratio in time, generating reproducible concentration waves of inducer. Furthermore, the chip includes a yeast trap, which allows for long duration imaging and tracking of yeast cells, while reducing clogging from excess growth. In addition, this new device is less complex, reducing the number of ports from eight to five. It was manufactured using standard photolithography methods, with the layout of the device drawn in Autocad (Autodesk) and the masks printed by CAD/Art Services.

A salient feature of this microfluidic device is the inclusion of staggered herringbone mixers (SHM), designed to cause corkscrew effects in convective fluid flow, which increases the surface area present for diffusive mixing. Increased surface area leads to reduced mixing times compared with simple diffusion across the interface of two laminar fluid streams. We maximized the flow velocity through this region, which limits the delay time for an input signal to reach the cell chamber while still ensuring adequate mixing. In contrast, the cell chamber region was designed to have a lower flow velocity by greatly increasing the channel width in this area. This lower velocity prevents cells from being forcibly removed from the cell trap region, while still allowing clearing of excess growth (Fig. S2*D*).

Another significant improvement in this unique design is in the dial-a-wave (DAW) junction region (Fig. S2*C*). The function of the DAW junction is to interface the fluid streams from the two input reservoirs with a minimum of diffusive mixing, because diffusion can lead to nonlinear changes in mixing ratios when the input pressures are altered. These nonlinearities are especially pronounced for unbalanced mixing ratios. Although the chip used in Bennett et al. (2) had a shunt network, the flow system was uneven with far more flow directed to the DAW junction outlet then the shunt network. Our current system is designed so that flow through each shunt and the DAW outlet is fairly constant under all mixing ratios. Moreover, the shunt architecture has been made more symmetrical, preventing gross changes in the fluid interface when mixing ratios are changed. The results of these changes can be seen in Fig. S2*E*, which demonstrates a linear system response as the applied pressure is increased.

In addition to the DAW junction, we have improved how external pressure is applied to the input syringes. The previous device made use of pneumatic valves to regulate this pressure; however, the valves were difficult to control reproducibly at the low working pressures (1–2 psi or 700–1,400 mm of water) required by this system. Furthermore, the pneumatic system was incapable of generating reproducible pressure steps of <1 mm of water. To simplify the application of external pressure, we have adopted a linear actuator system (RoboCylinder; Intelligent Actuator) to physically move the input syringes up and down, using gravity to apply different levels of hydrostatic pressure. We have found that hydrostatic pressure provides a more uniform and stable pressure source for microfluidics than most pneumatic systems can deliver. Moreover, the linear actuator system has a minimum step size of 10 μm, which is far superior to the previous pneumatic system and is at least one order of magnitude greater than the sensitivity of the device.

The competitive growth experiments described in Fig. 1 *C* and *D* were performed in our monster DAW chip, which has eight independent growth chambers of the type described in Fig. S2 in a single device. The other microfluidic experiments were done using the device diagrammed in Fig. S2.

Cell Cycle Analysis in Synchronous Cultures. To increase the dynamic range of the cell cycle experiments shown in Figs. 2*B* and 3*C*, which were done in asynchronous cultures, we repeated the analysis in synchronous cultures and monitored bud emergence as a marker for cell cycle entry. In these experiments, the culture was grown to midlog phase in galactose medium, arrested with nocodazole at the G2/M transition, and released into fresh galactose medium. The culture was allowed to synchronously move through mitosis while in galactose. We monitored mitotic progression by DAPI staining. Once ~80% of the population had reached G1, glucose was added and bud emergence was monitored by phase-contrast microscopy over time. As expected, in the WT strain the rate of bud emergence increased in cultures after glucose addition relative to those that continued in galactose medium. However, the stable (ST) strain had the same rate of bud emergence with and without glucose addition. These data support the results obtained from asynchronous cultures and are presented in Figs. S3*B* and S5*A*.

Characterization of the GAL1 ST Effect on Cell Cycle Dynamics. To identify the relevant aspects of *GAL1* repression, we assayed the cell cycle response in cells expressing a variety of tet-transactivator (tTA)-driven GAL1 alleles. We found that cells responded most readily to glucose if both forms of inhibition were used (addition of doxycyline to repress transcription and inclusion of the 5′-UTR for mRNA decay). However, in the absence of the 5′-UTR, transcriptional repression did not have an effect on the cell cycle response to glucose (Fig. S3*C*). This result indicated that the degradation of GAL1 mRNA has a stronger influence over the cell cycle response than transcriptional repression. The strength of the G1 delay caused by GAL1 mRNA was related to the level of GAL1 expression. A gal1Δ strain expressing the tTA-WT plasmid had a normal cell cycle response to glucose; however, this same plasmid caused a G1 delay in a strain that retained the endogenous GAL1 gene (Fig. S3*D*). This effect was even stronger when tTA-ST was used in place of tTA-WT. Therefore, both ST and tTA-WT produced a dominant negative G1 exit phenotype under these conditions. We next altered the ability of the overexpressed *GAL1* to absorb translational resources (Fig. S3 *E* and *F*). First, we deleted the sequence between two NdeI sites in the coding sequence of tTA-driven *GAL1* plasmid, which reduced the length of the

mRNA by about half (805 bp deleted). The ST version of this allele was a weaker inhibitor of the cell cycle response to glucose than the full-length ST allele, but still led to a significant G1 delay phenotype. To determine whether it was the length of the mRNA or simply the length of the ORF that was important, we inserted a frameshift mutation into the full-length ST allele to truncate the ORF at about the same position as the NdeI deletion. The phenotype caused by expression of this allele was similar to what we saw with the NdeI deletion mutant. These results suggest that it is the length of the ORF, but not necessarily the total length of the message, that is important for the phenotype. Because both truncated alleles lack the Gal1p kinase domain, these results also indicate that increased Gal1p activity is not the source of the cell cycle defect.

Whi5p-YFP Trajectories. The results of the Whi5p-YFP experiments indicate that there is a considerable difference between WT and ST strains with regard to G1 regulation (Fig. S4), which seems odd given the comparatively mild differences we measured by flow cytometry. However, it should be mentioned that tagging Whi5p with YFP appears to have made the cells overly sensitive to the expression of *GAL1*. First, these cells grew poorly in galactose relative to untagged strains, particularly under dynamic conditions. Furthermore, when we attempted to ectopically express *GAL1* from the tTA promoter, these cells arrested in G1 even when in glucose. Interpreted in the context of our hypothesis, this result suggests that the YFP tag interferes with the nuclear export of Whi5p and makes the cells sensitive to genetic changes that inhibit cell cycle entry. This caveat also suggests that the differences observed between WT and ST cells in this assay are likely exaggerated.

Polysome Distributions of GAL1 and CLN3. Yeast cells growing on an alternative carbon source respond to glucose by increasing global levels of protein synthesis. This global increase was detected in our polysome fractionation experiments. As illustrated in Fig. S5*C*, the amount of polysomes detected in lysates derived from galactose cultures increased after the addition of glucose. The polysome profiles of WT and ST cultures were comparable after glucose addition (Fig. S5*D*). When we compared the polysome distributions of GAL1 mRNA in cells before and after glucose addition (Fig. S5*E*), we found the distribution shifted toward the right in both WT and ST strains. As expected, the level of GAL1 mRNA was also decreased in WT strains in response to glucose, whereas it remained stable in ST cells. These results indicate that GAL1 transcripts have access to the additional ribosomes that are made available by the addition of glucose. CLN3 polysome distributions also shifted to the right with the addition of glucose in both WT and ST strains (Fig. S5*F*). However, the degree of change was reduced in ST cells relative to WT cells (Fig. 3). We can explain this observation in the context of the ribosome bank model illustrated in Fig. S8, which predicts that CLN3 mRNA does not acquire as many ribosomes in ST cells because it is still competing with the stable GAL1 transcripts.

Gal1p-CFP Accumulation Is Not Subject to Cell Cycle Position. Whereas overexpression of *CLN3* was able to hasten the response of ST cells to glucose, it had the unexpected consequence of slowing the accumulation of Gal1p-CFP in cells during growth in galactose. In the first 150 min in galactose, ST + CLN3 cells growing in a microfluidic device under dynamic conditions accumulated only 70% the amount of Gal1p-CFP compared to the ST or WT strains (Fig. S6*A*). qRT-PCR results showed that the level of GAL1 mRNA was not decreased in this strain, suggesting that the ability to efficiently produce Cln3p came at the expense of *GAL1* translation, not transcription. The ST + A315T-CLN3 cells were even more defective in GAL1 accumulation; many of them never displayed Gal1p-CFP expression, and those that did accumulated on average only 50% the WT level by 150 min. These results were surprising given the small increase in CLN3 mRNA that these cells had and considering that GAL1 mRNA is present at much higher concentrations than CLN3 when cells are in galactose. It appeared that the relationship of *GAL1* and *CLN3* was reciprocal and that excess CLN3 transcripts could interfere with the translation of GAL1 mRNA when cells were switched from glucose to galactose. We assayed the effect that increased CLN3 had on the growth of cells when they were first exposed to galactose and found that, whereas the ST + CLN3 strain grew normally, the ST + A315T-CLN3 strain was impaired (Fig. S6*B*). The level of Gal1p produced by ST + CLN3 (70%) appears to be sufficient for growth in galactose, whereas the amount produced by ST + A315T-CLN3 (50%) is not. This result suggests that there is a threshold level of Gal1p expression that is required for growth and that unregulated CLN3 translation inhibits the accumulation of Gal1p to sufficient levels.

We considered the possibility that GAL1 translation may be subject to cell cycle position and that, by decreasing the G1 fraction of the cell population, increased *CLN3* expression may have indirectly prevented Gal1p-CFP accumulation. However, the single cell trajectories do not support this hypothesis. WT cells began accumulating Gal1p-CFP at the same rate whether or not they were in G1 at the start of the galactose phase. In fact, in both WT and WT + CLN3, the cell cycle was responsive to Gal1p levels rather than the other way around. Upon being shifted to galactose medium, the cells paused wherever they were in the division cycle until Gal1p-CFP began to accumulate, at which point they resumed cell division (Fig. S6*C*). This point was reached within ~30 min for WT cells, but not until ~150 min in WT + CLN3 cells. These observations are consistent with there being a threshold level of Gal1p needed for cell division in galactose medium, rather than Gal1p synthesis being affected by cell cycle position. To confirm that *CLN3* expression was not affecting Gal1p accumulation through its effect on cell cycle position, we replaced the *CLN3* plasmid with one encoding a nonfunctional protein, Cln3p-ΔNLS (3). We found that Gal1p-CFP accumulated with dynamics and steady-state levels similar to what we observed in WT + CLN3 cells (Fig. S6*D*). These results support our model that it is the translation of CLN3 and not the activity of the protein product that prevents GAL1 translation.

WT Cells Growing in Static Galactose Do Not Respond Quickly to Glucose. In all of our dynamic growth experiments, we found that cells responded to glucose most readily if they had been exposed to glucose before. This observation suggests that there is some type of metabolic memory that allows cells to recognize or even to anticipate glucose if it has been available in the recent past. In fact, WT and ST cells usually responded to glucose with similar dynamics if the cultures were completely naive to glucose. This similarity was especially striking in the GAL1 mRNA decay curves, where both WT and ST transcripts were quite stable in cells that had never before experienced glucose in the medium (Fig. S7*B*). Consistent with this, WT Whi5p-YFP localization dynamics did not change in response to glucose when the cells had not been grown in glucose before (Fig. S7*C*). These results indicate that cells increase control of GAL1 mRNA levels and G1 regulation in response to dynamic growth conditions.

SI Materials and Methods

Plasmid and Strain Construction. The plasmids used in this study are described in Table S1. All cloned genes were amplified by PCR using primers to incorporate the necessary flanking restriction sites for subsequent ligations. The PCR reactions were carried out in a 50-μL volume containing 10 μL 5× Buffer HF, 1 μL 10 mM dNTP mix, 4 μL 10-μM primers (total), 25–50 ng DNA template, and 0.5 μL Phusion (NEB). PCR products were cloned into pCR-Blunt II TOPO vector (Invitrogen), according to the manufacturer's instructions. Amplified genes were then subcloned into appropri-

ate vectors, as follows: Construction of pBB14 was described in Bennett et al. (2). For pBB21, the *GAL1* coding region, starting with the first ATG, was amplified from pBB14 and subcloned into BamHI/NotI-digested pCM185. For pBB31, the genomic region upstream of *GAL1* (−300 to −1), including the 5′-UTR, was fused to the *YFP* gene using nested PCR; the fused product was subcloned into BamHI/NotI-digested pCM185. pBB53 is identical to pBB31, except that it lacks the *GAL1* sequence. To create pBB35, a fragment of *GAL1* (−1,000 to +450) was amplified by PCR from genomic DNA and subcloned into BamHI/XhoI of pBluscriptII-KS+. The *LEU2* marker was then ligated into the *GAL1* sequence upstream of the promoter between the EcoRI and ScaI sites. To create a randomized 5′-UTR_{GAL1} sequence, the first 100 bp upstream of *GAL1* was subjected to three rounds of randomization resulting in the following sequence:

5′ TAAAATAAAGCTAGTTATTATCATAGAAATTTCAAA
TGTTCATTCAGTCAATGTTTGATATTTTTATACCGA
TCTAACCAATAAACCTAAATAAGTCTAA 3′.

To make pBB36, the *GAL1* (+1 to +450) fragment was fused to the randomized 5′-UTR_{GAL1} sequence by nested PCR. The upstream *GAL1* (−1,000 to −100) fragment was then fused to *GAL1* (random to +450) in a second round of nested PCR. The *GAL1* (−1,000 to random to +450) fragment was then subcloned into BamHI/XhoI of pBluscriptII-KS+. The *TRP1* marker was ligated into the *GAL1* sequence upstream of the promoter between the EcoRI and ScaI sites. For integration, pBB35 and pBB36 were digested with DraI to release the *GAL1* fragment. pBB40 was made by amplifying *GAL10* including 700 bp of upstream sequence and ligating the PCR product into SpeI/SacII of pFA6a-KANMX6. To make pBB49, the *CLN3* coding region plus 900 bp of upstream sequence was amplified from genomic DNA and subcloned into SalI/NotI of pRS315. For pBB50, *A315T-CLN3* was amplified from A315T-pMT10 (generously provided by M. Polymenis) using the same primer pair and ligated into SalI/NotI of pRS315. pBB21-ΔNdeI (tTA-ST short) was made by digesting pBB21 with NdeI to release an 805-bp fragment and religating the plasmid. pBB21-i851C (tTA-ST shift) was made by site-directed mutagenesis using pBB21 as a template.

Yeast strains used in this study are described in Table S2. All yeast strains were made using standard methods for transformation and selection. The construction of K699-1cc2yv has been described previously. yBB114 and yBB115 were derived from K699-1cc2yv by integrating the DraI fragments released from pBB35 and pBB36, respectively. This integration resulted in separating *GAL10* from the GAL_{1-10} bidirectional promoter. To restore the *GAL10* promoter, pBB40 was linearized with StuI and integrated at the *GAL10* locus. yBB122 was derived from yBB115 by deleting *CLN3* with *hphNT1* (hygomycin B resistance), using standard one-step gene replacement.

Measurement of the 5′-UTR of GAL1 mRNA. To amplify the 5′-UTR of GAL1 mRNA, total RNA was prepared from ~3×10^7 K699 cells grown to log phase in synthetic medium with 2% galactose. The RLM-RACE kit (Qiagen) was then used according to the manufacturer's protocol for 5′ RACE. The gene-specific primers used were GAL1-EcoRI 5′ RACE 1 (5′ GAA TTC GGCGCAAAGCATATCAAAATCAATAGC 3′) and GAL1-EcoRI 5′ RACE 2 (5′ GAA TTC GGCGATCTAGCAACAAAATCCGG 3′). Reaction products were separated on a 2% Tris-acetate EDTA agarose gel and visualized by ethidium bromide staining (Fig. S1).

Flow Cytometry. To approximate the growth conditions of the microfluidics experiments, single colonies were inoculated into synthetic medium containing a mixture of glucose and galactose (1%/1%), grown to saturation overnight at 30 °C, diluted 1:100 in 20 mL fresh medium (1%/1%), and grown for 4 h. The cells were then pelleted and resuspended in 20 mL of medium containing 1% galactose and returned to growth at 30 °C for 4 h to induce the galactose network. At $t = 0$ min, 30 mL fresh medium containing 1.66% glucose was added directly to the galactose culture, to a final glucose concentration of 1%. Samples (5 mL) were collected every 5 min and processed for flow cytometry, as follows: Cells were briefly pelleted and resuspended in 2 mL 70% ethanol (EtOH) and stored at −20 °C overnight. The next day, the EtOH-fixed cells were rehydrated in 5 mL dH_2O, sonicated for 10 s at 40% power, and washed twice in 50 mM Tris, pH 8.0. Cell pellets were then resuspended in RNaseA (2 mg/mL) and incubated overnight at 37 °C. Cells were pelleted again, treated with pepsin (5 mg/mL) for 30 min at 37 °C, and then stained with propidium iodide (50 μg/mL) and run through a FACScan flow cytometer (Becton Dickinson). Flow cytometry data were analyzed using Gatelogic software. At any given time the culture consists of cells with one copy of the genome (1N) and those that have undergone DNA replication and possess two copies of the genome (2N). The size of the G1 fraction in each sample was estimated by measuring the percentage of cells in the 1N peak; the position of the G1 gate was kept constant for all samples. The reported results are averages of three independent experiments run in parallel.

To look at G1 progression in synchronous cultures (Figs. S3*B* and S5*A*), starting cultures were prepared in rich medium containing a mixture of glucose and galactose, diluted 1:100 in the same medium containing 2% galactose, and grown for 3 h. Nocodazole (15 μM final) was then added and the culture was incubated for another 2 h until >80% were arrested in G2/M. To release the cells, the nocodazole was removed with three 50-mL washes in sterile dH_2O. The cells were released into fresh medium containing 2% galactose. After 60 min, glucose was added to 2%. Samples were collected every 15 min after release and fixed in 70% EtOH. Fixed samples were sonicated and then stained with DAPI (5 ng/mL) in PBS. The mitotic fraction in each sample was determined by observing the shape of DAPI-stained nuclei. The budded and unbudded fractions were determined by phase-contrast microscopy.

Growth Rate Measurements in Dynamic Conditions. For Fig. S6*B*, single colonies were inoculated into synthetic medium containing a mixture of glucose and galactose (1%/1%), grown to saturation overnight at 30 °C, diluted 1:100 in 20 mL fresh medium (1%/1%), and grown for another 4 h. The cells were then pelleted and resuspended in 20 mL of the same medium containing 1% galactose and returned to growth at 30 °C. The density of each culture was then monitored and recorded as OD_{600} vs. time (hours). The graphs represent the growth curves of each strain normalized to 1.0 at time $t = 0$.

Polysome Fractionation. Single colonies were inoculated into synthetic medium containing a mixture of glucose and galactose (1%/1%), grown to saturation overnight at 30 °C, diluted 1:100 in 100 mL fresh medium (1%/1%), and grown for another 4 h. The cells were then pelleted and resuspended in 200 mL of the same medium containing 1% galactose and returned to growth at 30 °C until $OD_{600} = 0.4$ (typically 3 h). Half of the culture was then removed to a new flask containing cycloheximide (50 mg/mL final) and incubated at 30 °C for another 30 s. One volume of ice was then added directly to the culture and the cells were pelleted by centrifugation, washed once in cold polysome buffer (10 mM Tris·HCl, pH 7.5, 0.1 M NaCl, 30 mM $MgCl_2$, 50 mg/mL cycloheximide, 200 mg/mL heparin), pelleted again, and snap frozen in liquid nitrogen. Glucose (1% final) was then added to the remaining 100 mL of culture for 30 s, and the cells were treated and collected as before. Cell pellets were stored at −80 °C. Yeast polysomes were prepared and fractionated according to the protocol at http://openwetware.org/images/4/47/PlyriRNA.pdf. Polysomes were fractionated on 36 mL 10–47% sucrose gradients by

ultracentrifugation (27 K, 4 h, 4 °C) in an SW28 Beckman rotor. Polysome peaks were detected as A_{254} and recorded using a UA detector (ISCO) equipped with a digital chart recorder. Fractions (1 mL) were collected from the flow-through into an equal volume of cold 100% EtOH in 2-mL microfuge tubes. The fractions were stored overnight at −20 °C to allow the nucleic acids to precipitate. The precipitated nucleic acid was pelleted by centrifugation (14 K, 30 min, 4 °C) and the RNA was purified using the RNeasy kit (QIAGEN) following the manufacturer's protocol for RNA cleanup. Equal volumes of purified RNA (usually 10 μL) were used for qRT-PCR, as described above, to measure the relative amounts of GAL1 and CLN3 in the fractions of that region of the gradient containing ribosomes (usually fractions 17–32). The primer sequences are listed in Table S3.

FISH. For experiments shown in Fig. 4 *C* and *D*, a single colony of the parent strain, K699, was inoculated into synthetic medium containing a mixture of glucose and galactose (1%/1%), grown to saturation overnight at 30 °C, diluted 1:100 in 50 mL fresh medium (1%/1%), and grown for another 4 h. The cells were then pelleted and resuspended in 200 mL of the same medium containing 1% galactose and returned to growth at 30 °C for another 2.5 h. Cells were then fixed and hybridized according to the protocol at (http://www.singerlab.org/protocols). Fluorescent probes were made from double-stranded DNA representing the entire ORF of the target gene, amplified by PCR using gene-specific primers, and digested with restriction enzymes into fragments ≤1 kb. GAL1 sequence was cut with DraI and EcoRI, CLN3 was cut with HindIII and EcoRI, GAL2 was cut with EcoRI and AgeI, and ASH1 sequence was cut with HindIII. The digested DNA was then labeled with either TRITC or FITC using ULYSIS Nucleic Acid labeling kits (Alexa Fluor-546 and Alexa Fluor-488, respectively), according to the manufacturer's instructions (Invitrogen). Labeled probes were purified from unincorporated dye using the Qiaquick Nucleotide Removal kit (QIAGEN), following the manufacturer's instructions. The probes were denatured at 95 °C for 5 min before being added to the hybridization solution. Coverslips were mounted in Vectashield mounting medium with DAPI and allowed to solidify overnight at 4 °C. Image acquisition was performed on a Nikon Eclipse TI epifluorescent inverted microscope outfitted with fluorescence filter cubes for DAPI, TRITC, and FITC. Images were acquired using a Photometrics CoolSNAP HQ2 cooled CCD camera controlled by Nikon Elements software and processed in ImageJ. For experiments shown in Fig. 4*F*, a modified version of the FISH protocol for hybridization of yeast in solution found at http://web.mit.edu/biophysics/data.html was used. The following exceptions were made: We used the same fluorescent probes for GAL1 and CLN3 described above instead of the oligo probes recommended in the published protocol. We also included an extra high-stringency wash step in 2× SSC/40% formamide for 30 min at 37 °C to reduce background. Images were acquired and processed as described above. Quantitation represents results from 100–300 individual cells per hybridization.

1. Zacharioudakis I, Gligoris T, Tzamarias D (2007) A yeast catabolic enzyme controls transcriptional memory. *Curr Biol* 17:2041–2046.
2. Bennett MR, et al. (2008) Metabolic gene regulation in a dynamically changing environment. *Nature* 454:1119–1122.
3. Edgington NP, Futcher B (2001) Relationship between the function and the location of G1 cyclins in S. cerevisiae. *J Cell Sci* 114:4599–4611.

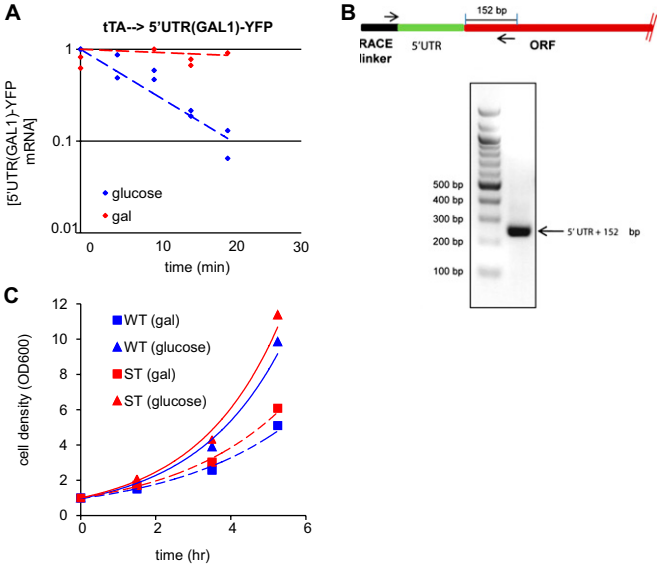

Fig. S1. (*A*) Decay of the tTA-driven 5′-*UTR*$_{GAL1}$-YFP fusion transcript in cells growing in glucose (blue) and galactose (red). The 5′-*UTR*$_{GAL1}$ destabilized the YFP transcript in glucose, but not galactose. (*B*) Results of RLM-RACE for GAL1 mRNA. In this experiment, a short RNA linker of known sequence was ligated to the 5′ end of mRNAs. After reverse transcription, the 5′ end of the gene of interest was amplified using a primer that anneals to the linker and a reverse primer that anneals inside the coding sequence. The diagram represents the position of the two primers in GAL1. The product of the PCR contains the 5′-UTR plus 152 bp of GAL1 sequence. (*C*) Growth rates of WT (blue) and ST (red) in 2% glucose (solid line) and 2% galactose (dashed line). The graph represents the growth curves of each strain normalized to 1 at time t = 0.

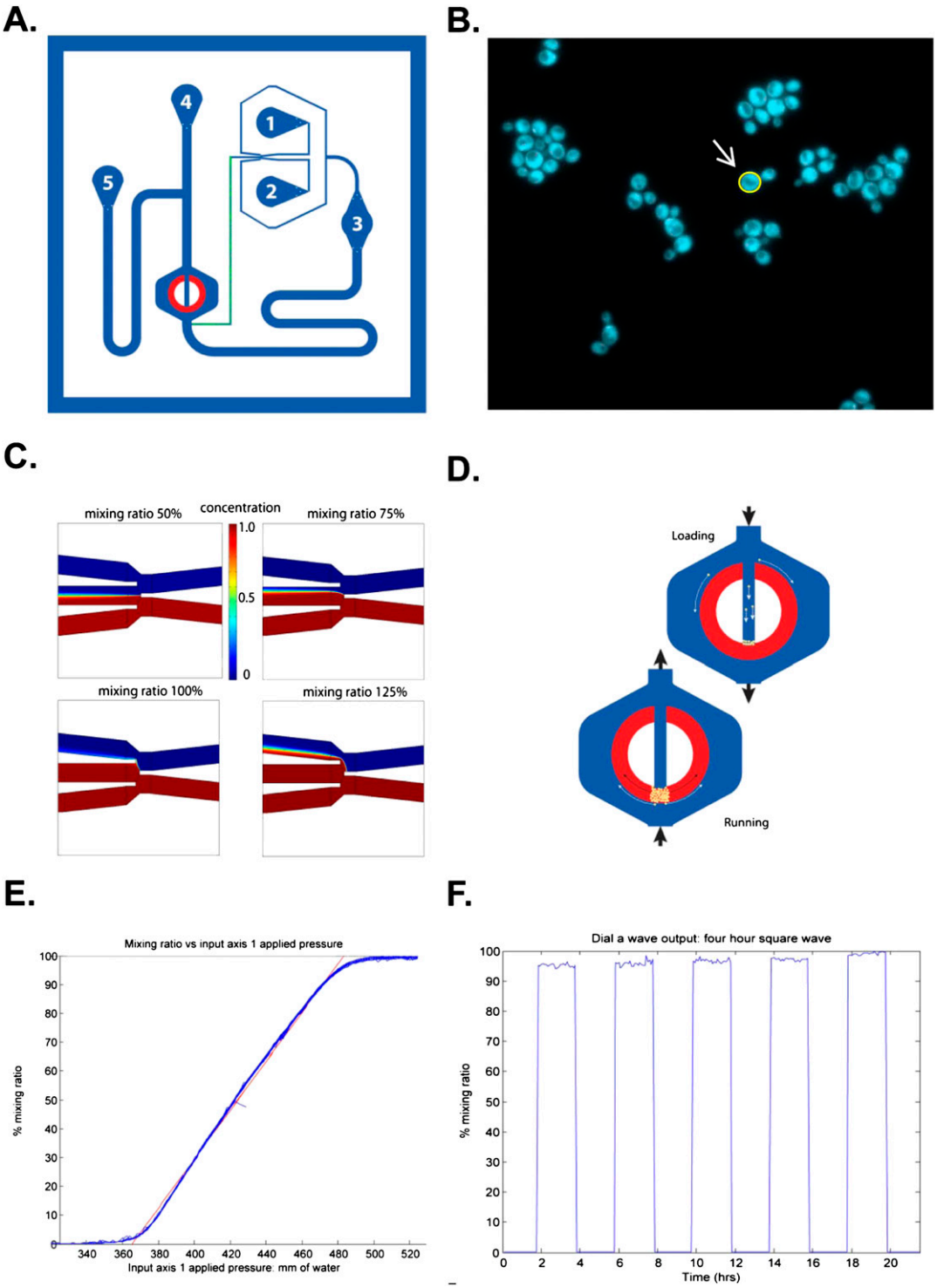

Fig. S2. (*A*) Schematic of the dial-a-wave (DAW) device described in the text. Ports 1 and 2 are the inputs for the DAW system. Port 3 is an outlet for the shunt network. Port 4 serves as an alternate waste port for the DAW system during the experiment. The device's primary flow network (dark blue) is 10 μm in height and the cell trap (red) is 3.5 μm in height. The region between the dial-a-wave junction and the cell chamber contains staggered herringbone mixers (green), which are 2 μm higher than the channel height. These mixers introduce a corkscrew effect into the fluid flow, which improves mixing. (*B*) Fluorescence micrograph of WT cells growing in the yeast trap of the DAW device. Cells are constricted to grow in a monolayer and are easily distinguished. To create single cell trajectories of Gal1p-CFP expression, individual cells are selected in ImageJ (yellow circle) and the pixel density inside the circle is measured. The frame is then advanced, the circle position is adjusted so that it remains directly over the same cell, and the process repeated. (*C*) Dial-a-wave junction region at different mixing ratios, as simulated using the program Comsol. The two inlets (from ports 1 and 2) are on the right side, and the outlet leading to the cell chamber is in the left center. (*D*) Graphic representing the cell chamber region during cell loading (*Upper*) and while the experiment is running (*Lower*). (*E*) Mixing ratio as the input pressure is increased on port 1. The red line represents the ideal linear response, which the system closely approximates. (*F*) Sample output of the DAW junction as measured near the cell trap. This is a square wave with a 4-h period and a 22-h duration.

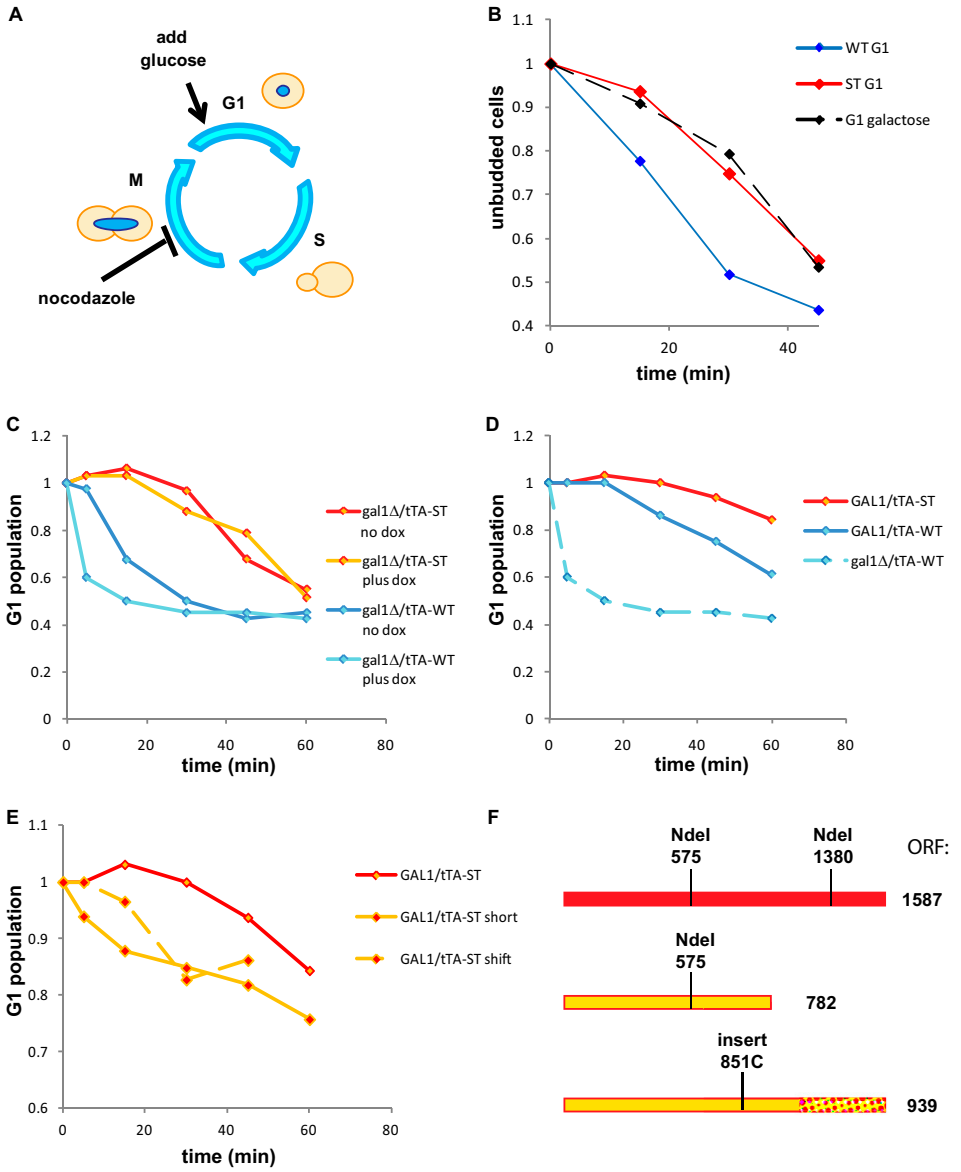

Fig. S3. (*A*) Diagram of experimental design for measuring the cell cycle response to glucose in synchronous populations. Cells were grown overnight in YEP medium with mixed glucose and galactose (1%/1%) and then diluted into fresh medium containing 2% galactose and grown to log phase. Nocodazole was then added to arrest cells at the G2/M transition. Arrested cells were released into fresh medium containing 2% galactose and allowed to synchronously pass through mitosis into G1. Mitotic progression was monitored by DAPI staining. When >80% of the cells were in G1, glucose was added to the medium. The transition of cells from G1 into S phase was monitored by bud counting. (*B*) Results of G1 progression after glucose addition for synchronous WT and ST cultures. The size of the G1 fraction over time after glucose addition is plotted. The WT cells (blue line) responded to glucose by increasing the rate of cell cycle entry. The ST cells (red line) did not respond to the addition of glucose and entered the cell cycle at the same rate as they did in galactose medium (black dashed line). (*C*) G1 fractions of asynchronous cultures plotted against time after glucose addition. The endogenous *GAL1* gene has been deleted in these strains and replaced with a tTA-driven plasmid encoding *GAL1* with (WT) or without (ST) its 5′-UTR. Transcription of *GAL1* was repressed by addition of doxycycline (dox) to the medium. Cells responded to glucose most rapidly when both levels of repression were used (tTA-WT plus dox). In the absence of glucose-mediated mRNA degradation (ST), transcriptional repression had little effect on the rate of the cell cycle response to glucose (tTA-ST plus dox vs. tTA-ST minus dox). (*D*) Cell cycle response to glucose plus dox in cells expressing tTA-GAL1 in addition to the endogenous *GAL1* gene. The excess WT-GAL1 expression caused a delay in the cell cycle response (blue line). Ectopic expression of ST-GAL1 in this background had a stronger effect (red line) than tTA-WT. The gal1Δ/tTA-WT curve from *C* is included for comparison. (*E* and *F*) Cell cycle response to glucose plus dox in cells expressing tTA-ST plasmids with truncated ORFs. The tTA-ST short allele has an 805-bp deletion from between two NdeI sites in the coding sequence. The tTA-ST shift allele has a frameshift mutation at position 851. Both types of mutations partially suppress the cell cycle delay phenotype of the tTA-ST allele. All graphs are representative results from at least two independent experiments run in triplicate.

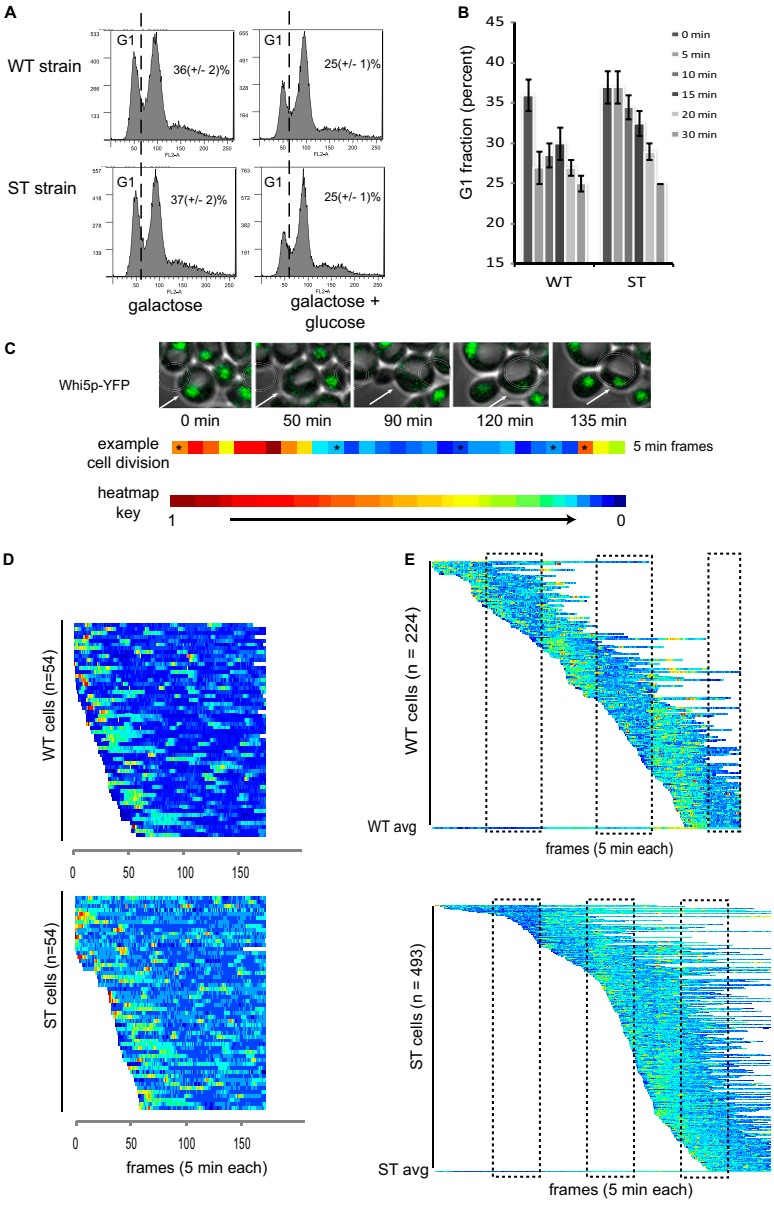

Fig. S4. (*A*) Cell cycle profiles of WT and ST cultures in galactose and galactose plus glucose, measured by flow cytometry. The cell cycle profiles of both WT and ST cultures indicate that each strain spent less time in G1 phase (represented by the indicated peak) when glucose was available. (*B*) Time course of cell cycle profiles for WT and ST cells after glucose addition. Batch cultures were grown to log phase in medium containing 2% galactose. At time $t = 0$ min, glucose was added to the culture to 2%. Cells were collected every 5 min, fixed, and processed for flow cytometry. (*C*) Increased global levels of protein synthesis in response to glucose leads to the production of Cln3p, the first cyclin in the cascade that drives the cell cycle. Cln3p enters the nucleus and causes Whi5p, an inhibitor of S phase, to be expelled from the nucleus. Cln3p also induces the expression of a number of cell cycle genes, such as CLN2, that promote S phase and reinforce the cytoplasmic retention of Whi5p. This feedback loop makes the entry into S phase irreversible and commits the cell to division. In this experiment, cells expressing Whi5p-YFP were grown in a microfluidic chemostat and imaged every 5 min using time-lapse fluorescence microscopy. Whi5p-YFP is easily detected in the nuclei of G1 cells, but the signal is weak when Whi5p is dispersed in the cytoplasm upon cell cycle entry. The heat map key shows the measured change in the level of maximum Whi5p-YFP signal for the indicated cell (white arrow) as it progressed through a division cycle. (*D*)Trajectories of Whi5p-YFP signal in single WT (*Upper*) and ST (*Lower*) cells growing in constant galactose expressed as heat maps. (*E*) Complete set of trajectories of Whi5p-YFP signal in single WT (*Upper*) and ST (*Lower*) cells growing in constant galactose with 4-h pulses of glucose every 4 h, expressed as heat maps. The dashed lines indicate periods during which glucose was present.

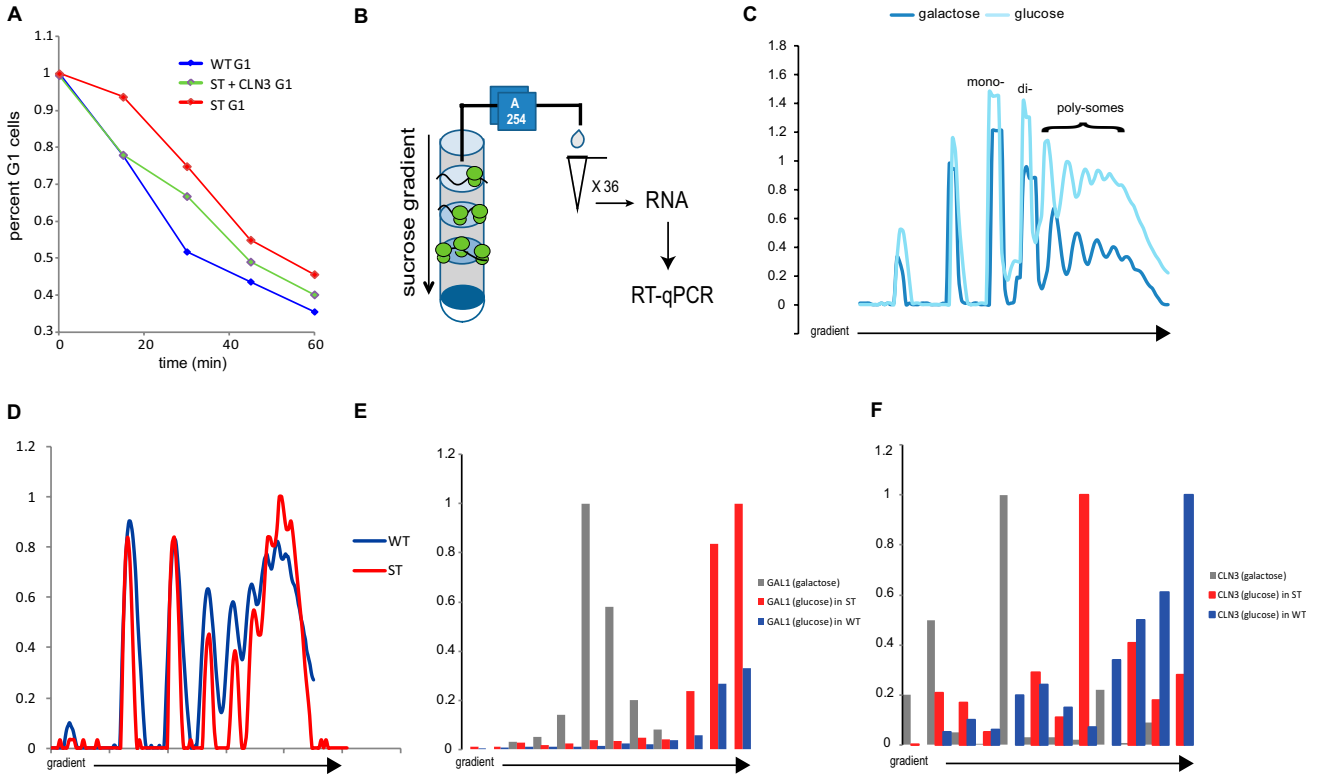

Fig. S5. (*A*) G1 fraction of synchronous cultures of WT and ST (from Fig. S3*A*) and ST + CLN3 cultures over time after glucose addition, measured as for Fig. S3*A*. (*B*) Schematic of polysome fractionation of WT and ST cells 30 s after glucose addition. Fractions were collected and analyzed by spectrophotometry (A_{254}) to detect ribosome complexes. Total RNA was prepared from each fraction and the relative level of CLN3 mRNA was measured by qRT-PCR. (*C*) Polysome profiles (A_{254}) of a WT culture growing in galactose for 3 h and the same culture 30 s after the addition of glucose. (*D*) Overlay of A_{254} traces for WT and ST cultures 30 s after glucose addition. (*E*) GAL1 polysome distribution in galactose and 30 s after glucose addition. After glucose addition, GAL1 mRNA shifts to the right for both WT and ST, indicating an increase in polysome association, consistent with the global rise in translation. As expected, the level of GAL1 mRNA decreases in the WT culture, but not in the ST culture. (*F*) CLN3 polysome distribution in galactose and 30 s after glucose addition. CLN3 mRNA shifts to the right in response to glucose; however, the induction of CLN3 translation in response to glucose is greater for WT than for ST cultures. In both *E* and *F* the galactose distributions shown are from the ST strain; there were no significant differences between WT and ST polysome distributions in galactose cultures.

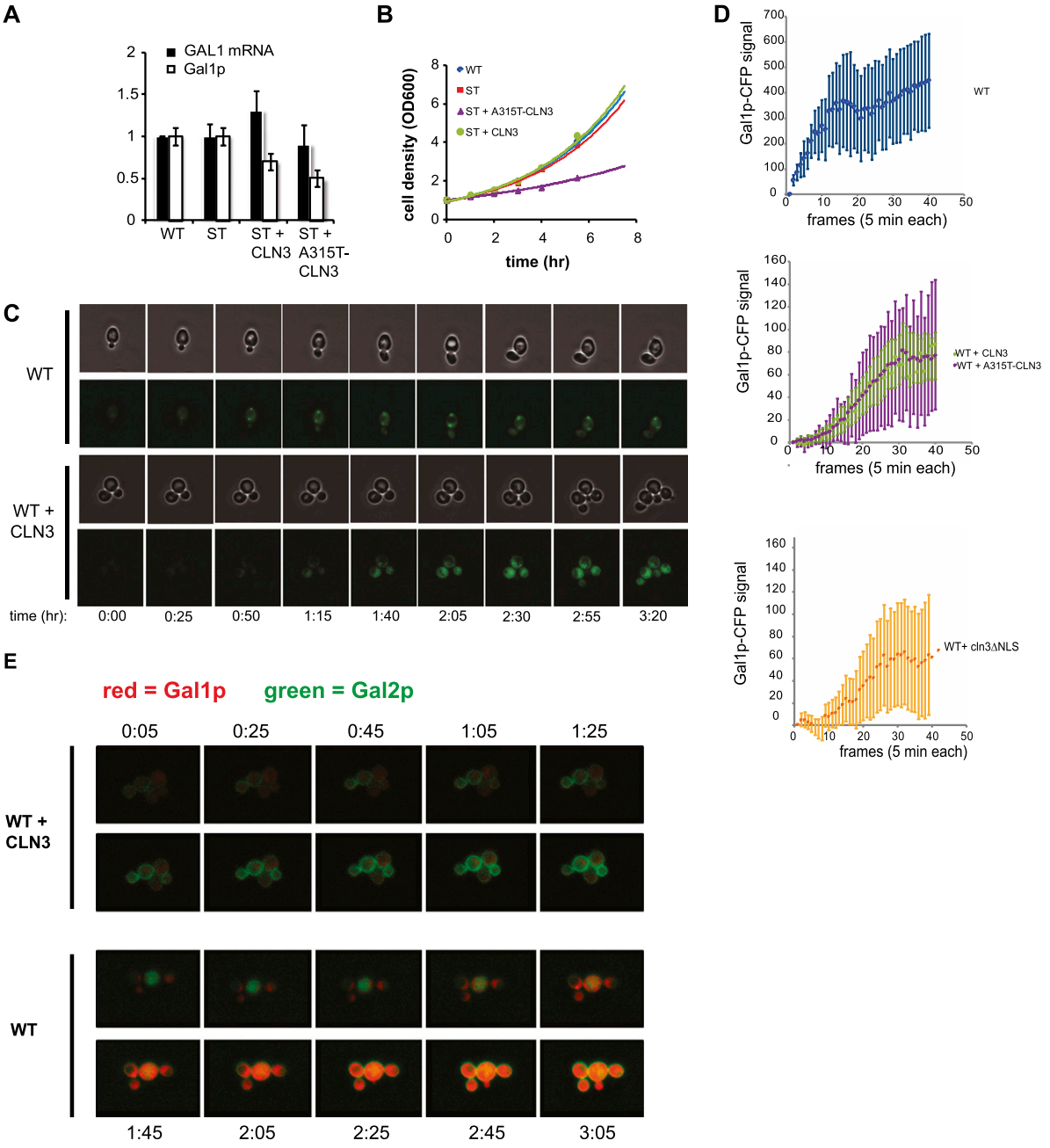

Fig. S6. Increased translation of CLN3 mRNA inhibits GAL1 translation. (*A*) Comparison of relative GAL1 mRNA levels and Gal1p levels in various strains, 2.5 h after cells were switched to growth in galactose. mRNA levels were measured in batch cultures by qRT-PCR; Gal1p levels are averaged from single-cell Gal1p-CFP trajectories derived from time-lapse microscopy experiments; error bars indicate ±1 SD. Increased expression of CLN3 led to a slower accumulation of Gal1p in ST cells, which could not be attributed to lower GAL1 mRNA levels. Increased CLN3 translation (A315T-CLN3) exacerbated this effect, indicating that the increased translation of CLN3 occurred at the expense of GAL1 translation. (*B*) Growth of various strains immediately after a switch to galactose in batch cultures. ST + A315T-CLN3 cells exhibited a growth defect when switched to growth on galactose. (*C*) Phase-contrast and fluorescence micrographs of representative WT and WT + CLN3 cells during the first 200 min of galactose induction. Upon being switched to growth in galactose, cells of both genotypes stalled wherever they were in their division cycle until Gal1p had accumulated. The contrasts of the fluorescence images are scaled independently for each individual trajectory. (*D*) Average Gal1p-CFP accumulation in WT (*Top*), WT + CLN3[A315T] (*Middle*), and WT + cln3-ΔNLS cells (*Bottom*), which overexpress a nonfunctional Cln3 protein, growing in a microfluidic chemostat; error bars are ±1 SD. (*E*) Time-lapse images of Gal1p-CFP and Gal2p-YFP induction in WT and WT + CLN3 cells. As shown in *D*, Gal1p-CFP accumulation is inhibited in WT + CLN3. In contrast, Gal2p-YFP accumulates at the same rate in both strains and is not affected by increased CLN3 expression.

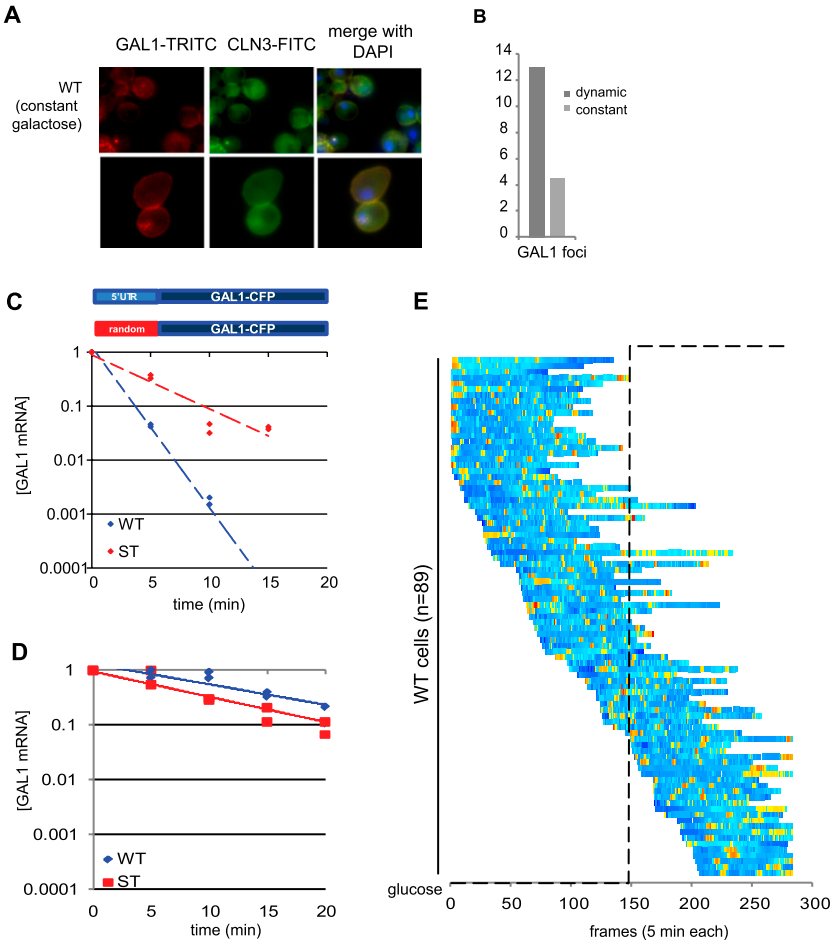

Fig. S7. (*A*) GAL1/CLN3 foci were rarely detected by FISH in WT cells that had been grown in galactose for 24 h. Cells with diffuse GAL1 mRNA staining (*Lower*) did not show colocalization with CLN3 mRNA. (*B*) Quantitation of GAL1 mRNA foci detected in WT cells grown under dynamic conditions or in constant galactose: combined results of two independent hybridization experiments. (*C*) GAL1 mRNA decay curves for WT and ST strains grown in dynamic conditions after glucose addition (from Fig. 1*C*). (*D*) GAL1 mRNA decay curves for WT and ST strains grown in static galactose conditions after glucose addition. Cells were grown overnight in medium containing 2% galactose and then diluted into the same medium 4 h before glucose was added. Following glucose addition, samples were collected every 5 min and processed for qRT-PCR, as described in Fig. 1*C*. (*E*) Whi5p-YFP trajectories of single WT cells grown in static galactose conditions. Cells were grown overnight in medium containing 2% galactose and then diluted into the same medium 4 h before being loaded into the microfluidic chip. Whi5-YFP localization was recorded over time by time-lapse microscopy, as described in Fig. 3. The dashed black line indicates the introduction of glucose into the growth medium. In contrast to what was observed in dynamic conditions, no change in G1 duration occurred after glucose addition. These results show that cells that are naive to glucose do not respond rapidly to the addition of glucose to the growth medium.

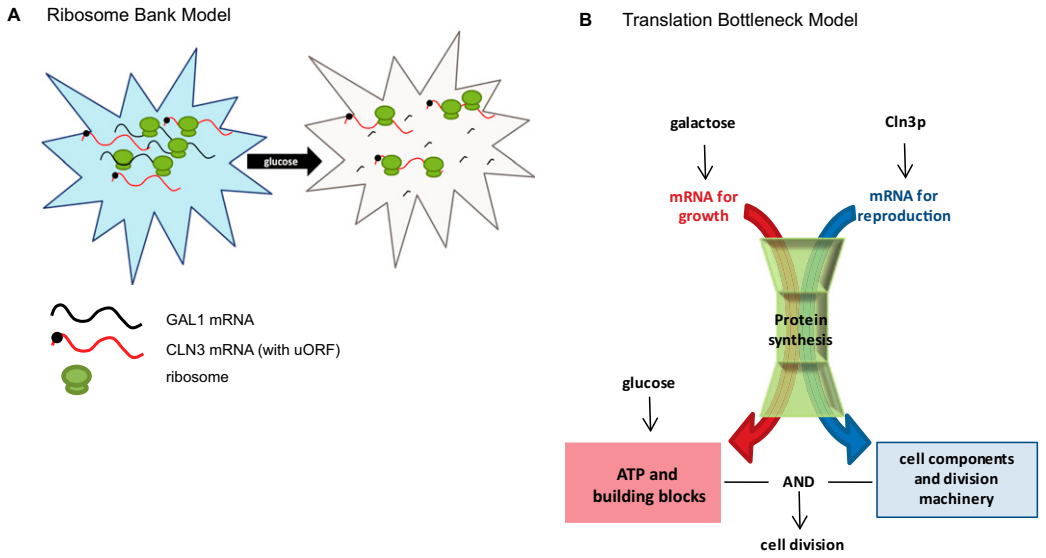

Fig. S8. (*A*) GAL1 and CLN3 transcripts are spatially coregulated when the environment dynamically switches between galactose and glucose. This observation indicates that these transcripts may compete for a local pool of translation components, explaining their mutual sensitivity to reciprocal changes in mRNA levels. The uORF on CLN3 messages (depicted as a black bead) makes GAL1 more competitive for translation when both types of mRNA are present. Therefore, in galactose GAL1 is strongly expressed and cell division is slowed through G1, allowing Gal1p to accumulate to high levels. When glucose becomes available, GAL1 transcripts are rapidly degraded, freeing up the ribosomes in the region, which CLN3 transcripts can take advantage of. This process leads to a concomitant rise in CLN3 translation and the induction of cell division. Therefore, the region of concentrated GAL1 transcripts acts like a ribosome bank for CLN3 in the event that glucose is suddenly added to the environment. (*B*) Model for how energy balance is achieved in different carbon sources. The spatial regulation of GAL1 and CLN3 mRNAs creates a translation bottleneck. Because both proteins that derive energy from carbon metabolism and those that assemble cell cycle components are required for cell division, a balance must be struck in the translation of mRNAs for each function. If the translation of cell cycle machinery increases, it does so at the expense of GAL gene translation, and cell division is delayed presumably because the cell cannot extract enough energy from galactose. On the other hand, if GAL1 mRNA persists in the cytoplasm after glucose becomes available, the translation of cell division components (CLN3) is hampered, and G1 is prolonged despite the availability of energy from the breakdown of glucose. Because glucose metabolism requires only the basal level of gene expression, this model may explain why it supports the fastest growth rate of yeast cells and may illustrate the biological basis of diauxic growth.

Table S1. Plasmids used in this study

Plasmid	Genotype	Vector
pBB14	*CEN; AmpR; TRP1; tTA; tetO7-GAL1* (including *5′*- and *3′-UTR*)	pCM185
pBB21	*CEN; AmpR; TRP1; tTA; tetO7-GAL1Δ5′-UTR* (including *3′-UTR*)	pCM185
pBB21-ΔNdeI	*CEN; AmpR; TRP1; tTA; tetO7-GAL1Δ5′-UTR* (including *3′-UTR*) and deletion from 575 to 1,380 in *GAL1 ORF*	pCM185
pBB21-i851C	*CEN; AmpR; TRP1; tTA; tetO7-GAL1Δ5′-UTR* (including *3′-UTR*) and frameshift mutation at 851 of *GAL1*	pCM185
pBB31	*CEN; AmpR; TRP1; tTA; tetO7-5′-UTR$_{GAL1}$-YFP*	pCM185
pBB35	*AmpR; LEU2-GAL1* (−1,000 to +450)	pBluescript-II
pBB36	*AmpR; TRP1-random 5′-UTR-GAL1* (−1,000 to +450)	pBluescript-II
pBB40	*AmpR; KANMX6; GAL10* (−700 to +3,500)	pFA6a-KANMX6
pBB49	*CEN; AmpR; LEU2; CLN3*	pRS315
pBB50	*CEN; AmpR; LEU2; A315T-CLN3*	pRS315
pBB53	*CEN; AmpR; TRP1; tTA; tetO7-YFP*	pCM185

Table S2. Strains used in this study

Number	Name	Genotype
K699	Parent	*MATa ade2-1 trp1-1 can1-100 leu2-3,112 his3-11,15 ura3*
yBB114	WT	*K699 GAL2::GAL2-YFP-spHIS5 GAL1::LEU2-GAL1(−1,000 to +450)-CFP-URA3 GAL10::pBB40*
yBB115	ST	*K699 GAL2::GAL2-YFP-spHIS5 GAL1::TRP1-random5′-UTR-GAL1(−1,000 to +450)-CFP-URA3 GAL10::pBB40*
yBB122	STΔcln3	*yBB115 cln3 hphNT1*
yBB125	WT	*K699 WHI5::YFP-HIS3, GAL1::LEU2-GAL1(−1,000 to +450) GAL10::pBB40*
yBB125-ST	ST	*K699 WHI5::YFP-HIS3 GAL1::TRP1-random5′-UTR-GAL1(−1,000 to +450)GAL10::pBB40*

Table S3. qPCR primers used in this study

Primer name	Primer sequence
GAL1 F	GGGCTTTAGTGTTGACGATGTCGCAC
GAL1 R	CAACCACCCCAGCCAGCTCCG
YFP F	CTGCTGACAAACAAAAGAATGGTATCAAAGCTAACTTC
YFP R	CCAGCAGCAGTAACAAATTCTAACAAGACCATGTGGTCTCTC
CLN2 F	CCATTCCTTCGCCCGCTTCCTCATCTC
CLN2 R	GGTTGCGTTATTGCTGTTAGGACCCGTG
CLN3 F	CCATTTGCCT TCACTCCAAC CTCATCTTCA
CLN3 R	TTAGAGATGGGGTGGTGGGTGTTAGTGGGC
ACT1 F	CAGAGCCCCAGAAGCTTTGTTCCATCC
ACT1 R	CTGGAGGAGCAATGATCTTGACCTTCATGG